Coordination Chemistry Reviews 253 (2009) 817–826

Contents lists available at ScienceDirect

Coordination Chemistry Reviews

journal homepage: www.elsevier.com/locate/ccr

Review

Are classical molecular mechanics calculations still useful in bioinorganic simulations?

Marc Zimmer

Chemistry Department, Connecticut College, New London CT06320, USA

Contents

ARTICLE INFO

Article history:
Received 5 February 2008
Accepted 14 April 2008
Available online 23 April 2008

Keywords:
Methyl coenzyme-M reductase
Urease
Molecular mechanics
Empirical force field calculations

ABSTRACT

There are currently no widely distributed molecular mechanics programs with inorganic force fields that allow the user to accurately model the structure of bioinorganic molecules without a prior parameterization of the metal coordination sphere. However, there are still times when the speed, accuracy and output of the calculations make inorganic molecular mechanics (MM) the method of choice. Bioinorganic molecular mechanical calculations are most commonly used to examine metalloproteins or parts of metalloproteins that are too large for analysis by QM/MM or DFT; to search large areas of conformational space; or in molecular dynamics. To illustrate the utility of inorganic molecular mechanics in bioinorganic chemistry, a brief review of simulations of bioinorganic compounds containing transitional metals published in the last 5 years is presented together with a computational analyses of methyl coenzyme-M reductase (MCR), which describes calculations that are too large for QM based methods, and urease, which is used as an example to illustrate how MM calculations can be used to sample large areas of conformational space. In the case of MCR, inorganic molecular mechanical conformational searches in conjunction with hole scans and normal-coordinate structural decomposition analysis are used to show how the protein matrix inhibits the non-planar deformations of the tetrapyrrole cofactor F430 and thereby changes its redox chemistry—an entatic effect. In our analysis of urease, inorganic molecular mechanical conformational searches were used to examine the conformational space available to the substrate and urea, and to examine potential mechanisms for its degradation.

E-mail address: mzim@conncoll.edu.

0010-8545/$ – see front matter © 2008 Elsevier B.V. All rights reserved.
doi:10.1016/j.ccr.2008.04.007

1. Introduction

Traditional inorganic molecular mechanics calculations still have a role in modeling biocoordination systems. This despite the fact that hybrid density functional theory (DFT) with the B3LYP exchange-correlation functional has been shown to be very useful in studies of transition metal complexes [1–5], and that QM/MM calculations of bioinorganic proteins are commonly published [6–10].

Most commercially available molecular mechanics (MM) programs are capable of routinely analyzing commonly occurring organic functionalities. Despite the fact that transition metal complexes were amongst the first molecules to be modeled by molecular mechanics [11,12], they play a minor role particularly if one contrasts their use in other disciplines, such as biochemistry. This is mainly due to the fact that transition metals have partially occupied d-orbitals [13] and the electronic structure of the metal does make a difference [2]. However, this might be changing as programs like LFMM [14,15] and SIBFA [16,17] continue developing and become more available and user friendly.

The main reason to use molecular mechanics calculations in the study of bioinorganic systems is that these calculations allow us to examine systems that are much too large for DFT simulations, and/or systems in which the conformational space available to the substrate in the active site of the metalloprotein cannot be adequately searched using QM/MM methods. Often inorganic molecular mechanics are run as quick and dirty supplements to other experimental methods, but with care they can be accurate and fast alternatives to QM/MM as shown in Deeth's study of oxidized type I copper proteins [15].

Here, we present a brief review of molecular mechanical analyses of bioinorganic systems published in the last 5 years together with some bioinorganic calculations our group has undertaken in the last 10 years. They are offered as an example to illustrate why at times inorganic MM calculations are the appropriate computational technique to be used in place of QM/MM or DFT calculations. Our computational analyses of methyl coenzyme-M reductase (MCR), which describes calculations that are too large for QM based methods, and of urease, which is used as an to illustrate how MM calculations can be used to sample large areas of conformational space, will be presented. The aim of this review is to use examples from the published literature to show that molecular mechanics calculations are useful in bioinorganic simulations. The focus is on potential uses of bioinorganic molecular mechanics, not on the theory and methods used.

1.1. Inorganic molecular mechanics

Inorganic, especially transition metal, molecular mechanics are not that straightforward. Special care needs to be taken due to the electronic effects of the partially filled d-orbitals. The calculations need to take into account the multiple geometries available to the metal (square planar, tetrahedral, octahedral, etc.), parameters for the correct charge and spin state need to be applied and, if present, the trans and Jahn–Teller effects also need to be considered.

Just like organic molecular mechanics, inorganic molecular mechanics uses mathematical equations to mimic the strain energy present in the compound being analyzed. In order to use the equations to calculate the total strain in the molecule, one needs to know the force constant (K) for all the bonds and bond angles in the molecule, all the ideal bond lengths (r°) and bond angles (θ°), the periodicity of the dihedral angles (n) and the barriers to their rotation (V). Also, the van der Waals parameters (A_{ij}, B_{ij}) between the ith and jth atoms are required to simulate the non-bonded van der Waals interactions, and finally, the point charges (q_i and q_j) and the effective dielectric constant (ε) are needed to model the electrostatic potential. There are four common ways of modeling valence angle deformations around transition metals within the molecular mechanics method, the electrostatic or ionic model, the valence force field model, electronically enhanced valence force field approach [14,18–22] and the points on a sphere (POS) approach [23–25].

In inorganic molecular mechanics force fields, these parameters are empirically derived, they have little or no relationship to physical observables, such as the stretching force constants determined by infra-red spectroscopy. Generally, they have been derived by fitting a number of crystal structures and are found in the parameter set of the MM program being used. Since the parameters are normally derived by fitting a series of crystal structures, one can view the calculated structure as a complex in an averaged crystal lattice, not as solvated or in the gas phase.

In all cases, the parameters have been derived for the specific force field employed, and are transferable from one molecule to another within the limits of the parameter set, but not between force fields. For example, it is not possible to take parameters derived for AMBER [26] and simply use them in another force field.

In organic (e.g. MM3 [27], MMFF [28]) and biological (e.g. AMBER [26], OPLS [29,30]) MM calculations, the force fields have been designed to model most known functionalities and therefore these force fields can be used to examine the vast majority of proteins and organic compounds. This is not always the case in inorganic MM calculations where practioners are either designing their own force fields to model many different metal, in different oxidation levels and with different coordination spheres (e.g. MOMEC [31–34]), or supplementing traditional force fields with routines that account for affects caused by partially occupied d-orbitals (e.g. adding ligand field effects into MOE with DommiMOE [14,15] or into SIBFA with SIBFA-LF [22]), or modify existing biological force fields to model a limited number of structurally similar metal complexes (e.g. using neural networks to derive supplemental MM2 parameters to model certain metalloporphyrins [35–37]).

1.2. Conformational searching in inorganic molecular mechanics

Most modern MM programs have a graphics interface which allows the user to enter the structure by drawing it or by reading its Cartesian coordinates; the strain energy of the molecule in this given conformation can then be minimized. However, the resulting conformation is not necessarily the lowest energy (or global energy minimum) structure. In fact, it is quite possible that the minimized structure can be significantly higher in energy than the global minimum and therefore it may be of little practical importance.

The aim of a conformational search is to find as many minima as possible, including the global minimum, and to compute the Boltzmann population. In doing such a search, a large number of high energy starting conformations are generated, minimized, compared with previously found conformers, and stored if they are unique. For a thorough search, the crude starting structures must span the entire potential energy surface; if only part of the surface is covered one cannot be sure that all important low-energy minima will be found. Ideally a grid or deterministic conformational search, in which the starting conformations cover all of the conformational space, should be conducted in all molecular simulations. However, for large and/or very flexible molecules, the cpu time required to explore the entire energy surface is prohibitive. It is more common to use stochastic or Monte Carlo methods, which employ a random element to generate starting geometries or to sample structures in a molecular dynamics run. Numerous conformational searching methods have been presented in the literature. Some of them have been designed for use on small cyclic and acyclic peptides

and organic molecules [38,39], while others were devised to search the conformational space available to small proteins [40–42], polymers [43] and carbohydrates [44]. Comparisons of different search methods have been published [45–47].

Conformational searches of transition metal compounds are complicated by the fact that inorganic complexes are often composed of multidentate ligands, resulting in many ring systems joined at the metal ion. Such metal ions can be found in a variety of coordination geometries (e.g. octahedral, trigonal prismatic, trigonal bipyramidal, square pyramidal, square planar, tetrahedral, etc.), and transition metal compounds often adopt geometrical isomers that are not available to organic compounds.

Using three test complexes, $[Co(dien)_2]^{3+}$, $[Co(dien)(dpt)]^{3+}$, and $[Co(hexamethylcyclam)(Cl_2)]^{3+}$, we investigated the ability of the random kick (Cartesian stochastic Monte Carlo search) method and the Monte Carlo dihedral and positional method to find all conformations and geometric isomers (dien, diethylenetriamine; dpt, di(3-aminopropyl)amine; tet-a, *meso*-5,5,7,12,12,14-hexamethyl-1,4,8,11-tetra-azacyclotetradecane; tet-b, *racemic*-5,5,7,12,12,14-hexamethyl-1,4,8,11-tetra-azacyclotetradecane). Both methods were found to be significant improvements on the typically used methods, in which all possible isomers were entered graphically and minimized individually. The major difficulty that was encountered in using Monte Carlo conformational searches was how to differentiate between the large number of similar conformations found [48].

Our recent unpublished work has shown that low-mode conformational searching [38,41] and mixed mode low-mode conformational searching methods are particularly efficient conformational search methods for examining small metallopeptides.

2. The case for bioinorganic molecular mechanics calculations

2.1. Bioinorganic mechanics calculations from the past 5 years

2.1.1. Molecular mechanics used to generate structures for QM/MM or DFT calculations

Matrix metalloproteinases (MMPs) are zinc-dependent endopeptidases that are capable of degrading extracellular matrix proteins and some bioactive molecules. MMP's can be divided into three domains—the pro-peptide, the catalytic domain and the haemopexin-like C-terminal domain, which is linked to the catalytic domain by a flexible hinge region. All MMPs are synthesized in the latent form and are secreted as proenzymes, which require extracellular activation. The pro-peptide domain must be removed before the enzyme is active; it is part of the so-called "cysteine switch," which contains a conserved cysteine residue that interacts with the zinc in the active site and prevents binding and cleavage of the substrate thereby keeping the enzyme in an inactive form. Zymogen activation is a major mechanism for the cellular control of MMP activity.

X-ray crystallographic structures of several MMP catalytic domains have shown that the active site contains a catalytically important Zn^{2+} ion, which is bound by three histidine residues.

In a very elegant paper, Mobashery and co-workers [49] used stopped-flow X-ray spectroscopy, molecular dynamics (MD) and QM/MM calculations to show that proteolytic cleavage destabilizes the pro-peptide domain conformation, thereby disrupting the cysteine zinc interaction, which results in an active enzyme form. A modified AMBER force field (with a bonded model for Zn(II) [50]) was used to run 10 different molecular dynamics simulations totally 75 ns. The crystal structure of pro-MMP9 (pdb ID: 1L6J) was used as the starting structure for the MD simulation, it has 415 amino acid residues. Data analysis revealed that one trajectory captured the entire activation event and sampling conformers showed them to be similar to those observed in their XAS experiments. Strategically sampled structures from this trajectory were used to provide seed structures for a subsequent QM/MM analysis. In the QM/MM geometry, optimization the zinc ion and all residues coordinated to it were treated at the QM level.

By combining MD simulations with QM/MM calculations, the authors were able to demonstrate the synergism among long-range protein conformational transitions, local structural rearrangements, and fine atomic events in the process of zymogen activation (MM and docking calculations have also been used to evaluate MMP inhibitors [51]).

2.1.2. QM/MM or DFT used to generate structures for MM calculations

Nitrogenase are responsible for biological nitrogen fixation. Besides fixing nitrogen nitrogenase also interact with a variety of other ligands, including acetylene, ethylene and carbon monoxide. Durrant [52] has used DFT calculations to determine the interactions of the iron and molybdenum sites in nitrogenase with either CO, C_2H_2 or C_2H_4. The resultant structures were then used to construct a ligated iron–molybdenum cofactor that was minimized in the nitrogenase protein matrix. The inorganic MM parameters used in these simulations are not very accurate, but then they do not need to be as the inorganic core is fixed using the DFT determined geometries. The work is based on previous DFT and MM calculations on nitrogen and hydrogen interactions with nitrogenase [53–55].

The base model used to examine the small molecule interactions with the central iron of the FeMoco was $[(HS)(H_2S)Fe(\mu\text{-}S)(\mu\text{-}NH_2)Fe(SH)(SH_2)]$, which has iron in both the Fe(II) and Fe(III) oxidation states. Two base models were used to simulate the Mo site in $[MS_3O_2]$ and in $[MoS_3ON]$, they were $[(HS)Fe(SH)_2Mo(SH)(OCH_2CO_2)]$ and $[Mo(SH)_3(OMe)(imH)]$. "The DFT optimized geometries were used to construct the appropriate ligands on the FeMoco, and the degree of van der Waals overlap with neighboring protein residues was measured before and after MM optimization of the protein side chains" [52].

The MM calculations were done with Chem-X and Insight II software. The standard Chem-X atom parameter set was modified to accommodate the FeMoco by including parameters for Fe and Mo, as follows. Three- and four-coordinate Fe and six-coordinate Mo atoms were defined, and bond lengths and angles were specified based on the crystal structure geometries. Chem-X geometry optimizations on FeMoco and its local protein environment were carried out keeping all FeMoco atoms, apart from the FeS3 moiety involved in substrate binding, and all protein backbone C and N atoms as a fixed restraint. Insight II calculations were performed on the subunit of crystal structure 1M1N, using the Discover module and cvff force field. During geometry optimizations large parts of the protein were fixed including the $-CH{=}CH_2$ group, the FeMoco core cluster, and homocitrate. Partial atomic charges were specified based on the output from the DFT calculations.

These calculations were used to rationalize the mutagenesis data that implicated C_2H_2 reduction on a central face of the FeMoco; the production of *cis*- versus *trans*-CHD=CHD; the production of C_2H_4 versus C_2H_6 from C_2H_2; and the reduction cycle determined for C_2H_2. This catalytic cycle is fully compatible with that proposed for N_2 and H^+ reduction suggested in prior work by the same authors [53,54].

2.1.3. MM calculations used to interpret spectroscopic results

- Parak and co-workers [56] combined a molecular mechanical conformational search of the copper(II) binding region in the full-length human prion protein with simulated EPR, ENDOR and

EXAFS spectra to derive a new model for the binding region. The calculations described in this paper are very ambitious as they start from an extend random coil structure of the human full-length cellular prion protein with copper covalently bound to the N_δ of His69 and His85. A simulated annealing protocol developed in-house was used with a modified CHARMM22 force field to generate 5000 conformations [57]. This number was whittled down to 100 structures by the use of selection rules that removed structures that were incompatible with their EPR, ENDOR and EXAFS results. EXAFS spectra were simulated on the basis of the 100 structures. The structures responsible for the five best EXAFS simulations were selected for further refinement and comparison with spectroscopic data, and a final best model chosen. The simulated spectra of the calculated structures fully agree with the experimentally obtained EPR, ENDOR and EXAFS spectra, resulting in a reliable model for the copper(II) complex that differs significantly to those obtained previously for shorter peptides.

In a further very similar paper [58], the same authors use their results described in the preceding paragraph to find the configuration that produces the best comparison between simulated and experimentally obtain spectra of an octapeptide that corresponds to residues 60–67 of full-length human prion protein bound to copper(II). Particular emphasis is put on simulating the superhyperfine interaction of the octapeptide.

- Deletion experiments have shown that a four tandem repeat of the octapeptide PHGGGWGQ in prion protein preferably binds copper(II) over other metals. It has been shown that the four tandem repeat is essential for copper(II) reduction, that the redox potential is pH dependent, and that the tryptophan residues are critically important to the reduction [59]. To understand the role of the tryptophan Muira et al. undertook molecular mechanical calculations. A starting structure of a 1:1 copper/octapeptide tetramer complex was graphically created, minimized, subjected to 100 short simulated annealing sequences and minimized again. I would be very surprised if this very limited conformational search would find the global minimum structure. The copper(II) parameters were not reported, nor was their origin given.
- In an attempt to understand the effects of the protein environment on the reduction potential of electron transfer proteins Ichiye and co-workers [60] have examined crystal structures, undertaken MM simulations and sequence analyses of wild-type and mutant *Clostridium pasteurianum* rubredoxin. In an earlier study, they found that mutations of residue 44 from alanine to valine affect the redox potential of rubredoxin [61]. Upon mutating residue 44 to other non-polar residues they found that there is no side-chain size/redox potential relation. CHARMM25 was used with a CHARMM19 modified force field that includes parameters for the iron–sulfur site [62] to energy minimize and do MD simulations of the rubredoxin (pdb ID: 5RXN). The energy minimizations were found to be useful in identifying changes in the protein structure caused by the mutations, while the MD simulations were more useful in identifying conformational variability and solvent penetration. Overall the combined analysis of the glycine, alanine, isoleucine and leucine mutations at residue 44 indicated that the difference in backbone position and the water penetration, rather than the side-chain size were the two structural determinants responsible for the difference in reduction potentials between the Cp rubredoxin mutants.

2.1.4. Metalloprotein folding and de novo structure prediction

One of the most challenging and interesting areas of computational chemistry is the *de novo* structure prediction. However, simulations of peptide and protein folding in metalloproteins are rare. Some of the reasons for this are that during folding charge transfer can occur between the metal and ligating atoms, and the formation and cleavage of metal–ligand bonds can occur. Typically these occurrences are best modeled with QM, however, the computational demands of such QM simulations are not yet feasible. Here, I will describe some MM based attempts to model folding in metalloproteins.

- Gresh and Derreumaux [63] have developed a hierarchical procedure for finding the most favored folding geometries of a 18-residue zinc finger found in the HIV-1 nucleocapsid protein. The procedure consisted of the following three steps: (1) determination of the lowest-energy topologies by global optimization of a potential of mean force using a kinetic Monte Carlo (MC) procedure and a simplified chain representation [64,65]. (2) Clustering of the aforementioned conformations. (3) Post-processing of selected conformations by the SIBFA force field [16]. The resultant structures deviated by between 2.2 and 3.5 Å from NMR conformations and the energies were validated by DFT calculations.
- Wang and co-workers have also used a polarizable force field to examine metal-coupled folding in the second finger of the human transcription factor Sp1 [66]. Understanding the folding and stability of the zinc fingers is important in designing new zinc finger motifs and in treating diseases associated disruption of the zinc finger structure. Before publication of this paper in 2008, it was unclear whether zinc(II) induces peptide folding, binds at an early stage of folding or just binds at the end of folding and stabilizes the native structure. By implicitly accounting for the effects of the charge transfers that occur between zinc(II) and its ligands as well as for protonation/deprotonation effects in the classical MD model and performing intensive all-atom simulation for the peptides with and without zinc binding they were able to show that the zinc ion binds the peptide at an early stage of folding and modulates the folding and stabilizes the α-hairpin and α-helical components. The AMBER8 package was used with a modified AMBER ff03 force field.
- Metallothioneins fold into their three-dimensional structure upon metal chelation. Mammalian metallothionein binds divalent metal ions, such as cadmium(II) and zinc(II) forming M3S9 metal-cysteine clusters with the N-terminal β-domain and M4S11 clusters with C-terminal α-domain. The fully metallated structures have been characterized by X-ray crystallography, NMR and X-ray absorption spectroscopy, however, the structures of partially metallated and apo metallothioneins are not known. Molecular dynamics have been used to study the structural consequences of metallation and demetallation of the individual domains of metallothionein [67–69]. A MM3 force field with parameters derived from rabbit liver metallothionein-2 and small model compounds of the Zn and Cd thiolate clusters was used. The simulation of the demetallation described next is typical of all the rather localized and brief conformational searches found in these papers. Demetallation involved "deletion of the selected metal ions followed by protonation of the terminal-bound cysteinyl sulfur atoms that were released by the metal ions. The bridging cysteinyl sulfurs became terminal for the remaining Cd atoms. The demetallated conformation was minimized (MM3) before molecular dynamics (MM3/MD) calculation. Unless otherwise specified, the optimized structure was modeled for 250 ps at 300 K followed by minimization (MM3) of the final 250 ps conformation. This energy-minimized structure was then annealed (relaxed) at 100 K for 100 ps before obtaining the final energy-minimized protein conformation [68].

2.1.5. MM simulations to predict the structural consequences of mutations in metalloproteins

Although not a trivial task, it is a lot easier to use bioinorganic molecular mechanics to find the structural consequences of selected point mutations in known metalloprotein structures, than it is to model metalloprotein folding or predict protein structure de novo.

- Having modeled the interaction of nitrogenase with CO, C_2H_2 or C_2H_4 (see Section 2.1.2) Durrant et al. combined bioinorganic molecular mechanics with nitrogenase activity studies to determine the effect of substitutions at α-Lys-426 [70]. The activity studies showed that substitutions at α-Lys-426 can impair nitrogenases ability to reduce N2 without affecting its acetylene-reducing ability. These results were interpreted in light of a molecular mechanics study of the wild-type and mutant MoFe-nitrogenase in an open and a closed form. In the closed form the homocitrate coordinates the Mo as seen in the X-ray crystal structures, and in the open form the Mo–O bond to the homocitrate β-carboxylate group has been broken and the homocitrate has rotated to allow coordination of nitrogen at the molybdenum. The computational details were similar to those described in Section 2.1.2.
- In a rather ambitious study, Bongini et al. have attempted to use molecular mechanical methods to design small peptides that selectively bind aluminum. In a preliminary report [71] they describe how they use a peptide fragment with an EF-hand motif from troponin C as their starting structure, and how the InsightII program was used with charmmPLR forcefield parameters to find potential mutants that would stabilize the relatively small Al^{3+} ion.

2.1.6. Tetrapyrroles

- Oda et al. have used DFT calculations of cytochrome P450 model systems to establish some AMBER force-field parameters [72], while Marques and co-workers have derived MM2 force field parameters for Sc(III) [37], Zn(II) [36], Mn(II), Mn(III), Mn(IV), Mn(V), Co(I), Co(II), Co(III), Ni(II) and Cu(II) porphyrins [35] from solid state structures. Marques et al. have also used their cobalamin modified MM2 force field [73,74] to determine consensus structures based on NMR constrained MD simulations [75] and to find the effect of axial Co–N bond compression [76].
- Coenzyme F430 is a nickel porphinoid complex found in methyl coenzyme M reductase, see Section 2.2.1 and Fig. 1. X-ray crystal structures of the enzyme show that the nickel is penta- or hexacoordinated. Bauer and Jaun [77] have designed derivatives of coenzyme F430 with a coordinating group, such as an imadzole, attached via a linker to one of the propanoic acid side chain. They used molecular mechanics and conformational searching methods to find a sidechain and linker that would optimally bring the coordinating ligand from one side of the corphinoid, and then checked their results by synthesizing the derivatized F430 and determining its solution structure [77,78].
- Niketic and Rasmussen developed the Consistent Force Field (CFF) program [79] in the mid seventies, it has parameters for metal ions and Niketic has published a steady stream of papers dealing with small inorganic complexes [80–85]. In 2004, he published an analysis of tetrabromotetraphenylporphyrins bound to Ni(II) and Tb(III) [86]. He used the CFF to determine the non-planar deformations of the porphyrins and categorized them using normal-coordinate structural decomposition (NSD). In place of a conformational search the energy minimizations were initiated from starting structures with each of the most commonly occurring non-planar deformations (*dom, sad, wav* and *ruf*). Similar techniques were used to model the non-planar deformations of nickel(II) octaethylporphyrin adsorbed onto a graphite surface [87]. In place of a conformational search geometry, optimizations were carried out for 43 conformations of 28 distinct conformers of nickel(II) octaethylporphyrin. This works because the conformational space available to the prophyrin is limited and sampling the available conformational space by graphically creating all possible conformations and minimizing them is adequate.

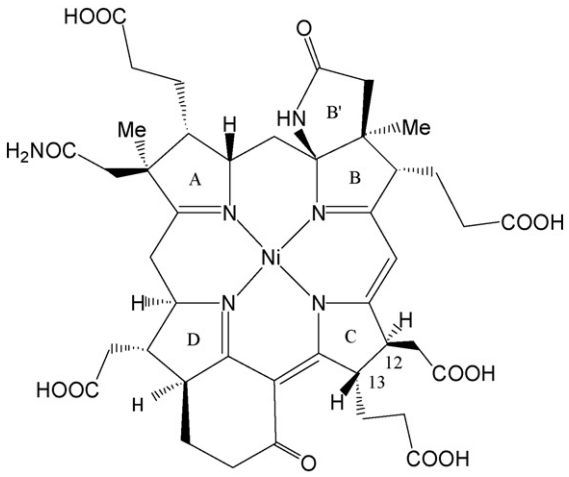

Fig. 1. The structure of cofactor F430. Diepimerization occurs at positions 12 and 13.

2.1.7. DNA

Modeling DNA is not a simple undertaking, as it is a flexible and highly charged molecule. Simulating the effects of metal binding on the DNA helical parameters, sugar pucker, hydration, hydrogen-bonding and base twisting are even more problematic. There are two approaches to modeling metallo-DNA complexes, a rigorous approach in which the parameters are carefully derived to accurately model very specific metal–DNA interactions (e.g. Spiegel et al. [88] and Gresh et al. [89]), and a more common approach in which the molecular mechanics calculations can be considered as not much more than glorified model building. This second approach may not be as accurate as the first approach, but can nevertheless be useful if the results are not overinterpreted.

- Hybrid quantum classical molecular dynamics simulations (QM/MM MD) of azole-bridged platinum anticancer drugs have revealed local deformations at the DNA binding site [90]. However, since the time-scales of the drug induced DNA distortions cannot be addressed by QM/MM MD, Spiegel et al. have developed AMBER parm98 parameters by force matching and have conducted 10 ns MD simulations of the diplatinated DNA decamer [88].
- SIBFA polarizable molecular mechanics [91,92], polarizable and non-polarizable AMBER, ab initio and DFT calculations of the binding of hydrated Zn(II) and Mg(II) cations to 5′-guanosine monophosphate were compared in a study by Gresh et al. [89]. A variety of mono- and bi-dendate binding modes and sugar puckers were considered. The SIBFA polarizable molecular mechanics calculation results agree with those obtained by DFT computations. One of the advantages of using SIBFA over standard MM programs is that the polarizable force fields can be used to determine the interaction energy and separate it into charge transfer, intra- and intermolecular polarization interactions. Thus, the authors were able to establish the effects of charge fluctuations

that occur upon binding Zn(II) and Mg(II) at different sites on 5′-guanosine monophosphate.
- Metallointercalators selectively bind both normal and sheared DNA. Xiong et al. have modeled the site selective binding of two stereoisomers of a ruthenium bipyridine complex to both a normal and sheared decamer of DNA. The intercalating moiety of the ruthenium complexes was graphically docked parallel to the base pair planes and just out of the DNA helix for all base pairs except the terminal ones. Then the ruthenium complex was intercalated further into the DNA, minimizing the every 0.2 nm. Major groove intercalation was preferred over minor groove and the complexes displayed weak enantioselectivity.
- The DNA binding affinity, solvatochromism and cytotoxicity of four mixed-ligand copper(II) complexes has been reported by El-Ayaan et al. and the results have been interpreted using a molecular mechanics and molecular dynamics simulation [93].
- To supplement their calorimetry and circular dichroism studies of a DNA triplex containing a ferrocenemethyl-thymidine residue in the third strand Petraccone et al. have used molecular mechanics [94]. However, the details of the calculations are sparse.

2.2. Two examples from our own research

In the following two examples, I hope to show how bioinorganic MM calculations were used to get results that are not accessible to higher level techniques. Our analyses of methyl coenzyme-M reductase and urease are presented in order to show the reader some applications of bioinorganic molecular mechanics that are not easily done by using QM/MM or DFT calculations. This review is not focused on the calculations themselves, for details of the calculations consult the original publications. It should be noted that in all our calculations we have used force field parameters derived from solid state structures [95,96], this is an important limitation. The conformations resulting from these calculations are "crystal averaged" structures, they are very good geometric approximations of the solid state structure, but much like crystal structures, they do not provide any electronic information. One can therefore consider the resulting conformation as that of a complex in an averaged crystal lattice, not as solvated or in the gas phase. If the complex being investigated differs significantly from the structures used to derive the parameters, the results will be of low quality.

2.2.1. Methyl coenzyme-M reductase

Anaerobic bacteria produce four hundred million tons of methane annually. About 45 million metric tons of the methane escape into the troposphere and significantly contribute to the greenhouse effect [97]. Methyl coenzyme-M reductase (MCR) is a key enzyme common to all methane producing pathogens. It catalyzes the last step of methanogenesis.

Crystal structures of MCR from *Methanobacterium marburgensis, Methanosarcina barkeri* and *Methanopyrus kandleri* have been published [98–100]. Each MCR is composed of three subunits in a $(\alpha\beta\gamma)_2$ structure and contains two non-covalently bound molecules of cofactor F430 that are located about 50 Å from each other. This unusual nickel tetrahydrocorphinoid cofactor, Fig. 1, is most likely the active site of MCR [101].

2.2.1.1. Free cofactor F430. The cofactor F430 is held in place within the protein (MCR) via hydrogen-bonding to the partially negatively charged carboxylate groups of the Ni-porphrinoid [102].

Free cofactor F430 is thermally unstable, it first epimerizes to 13-epi F430 and then in a second epimerization to 12,13-diepi F430 [103]. Because of problems in the purification procedure, the crystal structure of free F430 has not been solved, however, the structure of a methanolated derivative, 12,13-diepi F430M, has been published [104]. The corphinoid ring is significantly deformed from planarity. In fact it is one of the most non-planar tetrapyrroles in the Cambridge Structural Database [105] and a substantial conformational search is required to find the solid state 12,13-diepi F430M structure from a planar12,13-diepi F430M starting structure [106]. Based on graphical diepimerization of free 12,13-diepi F430M to native F430 and a subsequent conformational search, we predicted that the diepimerization will involve a large conformational change from a ruffled geometry to saddled geometry, see Fig. 2 [106]. Cofactor F430 has a complex potential energy surface, which is the main reason we have used MM calculations. The speed of the MM calculations allows us to undertake thorough conformational searches and to find the conformations available to cofactor F430.

Non-planar distortions are important, numerous studies have shown that they have a significant effect on the chemistries of tetrapyrrole complexes [107]. It has been suggested that the non-planar deformations observed in photosynthetic proteins are responsible for the photophysical and redox properties of chlorophyll pigments [108]. Non-planar porphyrins are easier to oxidize than planar porphyrins [108–110]. Excited state lifetimes of porphyrins are influenced by non-planar deformations [109,110] as are the axial ligand affinities [111].

MM calculations and their ability to do large scale conformational searches were our method of choice in studying free cofactor F430 because cofactor F430 is very flexible, it diepimerizes, which involves a conformational change, and the different conformations effect the chemistry of the nickel ion.

2.2.1.2. Cofactor F430 in methyl coenzyme-M reductase. Resonance Raman studies have shown that cofactor F430 undergoes a significant conformational change when it binds MCR [112]. We have therefore used a combination of molecular mechanics calculations, cluster and hole-size analysis to examine the effect of methyl coenzyme-M reductase (MCR) on the non-planar deformations of coenzyme F430 [113,114].

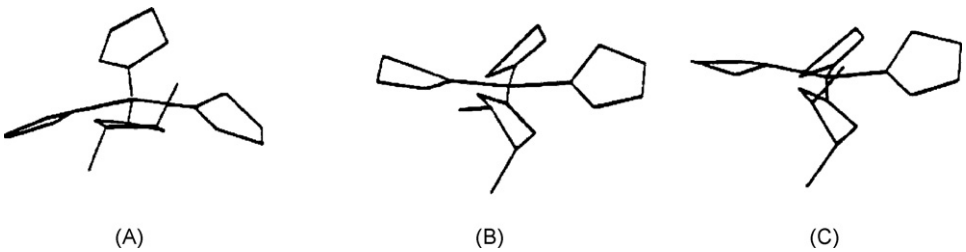

Fig. 2. Conformation of the pyrrole rings in F430 (A, saddled), 13-epi F430 (B, ruffled) and 12,13-diepi F430 (C, ruffled). Carbons 12 and 13 with non-hydrogen substituents shown in foreground. At thermodynamic equilibrium, 4% of free cofactor F430, 8% of 13-epi-F430, and 88% of the most stable isomer 12,13-diepi-F430 are found. This figure has previously appeared in reference [106].

Most tetrapyrrole structures in the CSD are non-planar with deformations occurring in a direction perpendicular to the tetraaza plane. They can be classified into six classes. These are based on simple symmetric deformations, one of each out-of-plane symmetry classification of the (D4h) point group of the square-planar macrocycle. We have used a normal-coordinate structural decomposition procedure [115] to characterize and quantify the MM determined F430 non-planar deformations in MCR. The method determines the out-of-plane distortions in terms of the equivalent distortions along the lowest-frequency normal coordinates of the porphyrin [116].

Although free 12,13-diepi F430 has a lower energy conformation than free F430, the protein restraints exerted by MCR are responsible for F430 having a lower energy conformation than the 12,13-diepimer in MCR. According to the NSD analysis, the crystal structure of free diepimerized F430M is highly distorted. In MCR, the protein prevents 12,13-diepi F430 from undergoing non-planar deformations and therefore MCR favors F430 over the 12,13-diepimeric form [113]. The strain imposed on 12,13-diepi F430 in the protein is so large that although 88% of free F430 is found in the diepimeric form, none of the diepimeric form is found in MCR. This is of significance since the two forms have different chemistries.

In order to determine the effect of the protein on the non-planar deformations of the tetrahydrocorphinoid F430 molecular mechanics simulations and conformational searches of free cofactor F430 and cofactor F430 in MCR were carried out. The effect of the protein on the conformation of F430 can be seen by comparing the energy-minimized conformations of F430 within MCR and free F430, and by plotting the changes that occur in the B2u(sad) and B2u(ruf) deformations, see Fig. 3 (note the large change in saddling and ruffling that is only determined after undertaking a conformational search, i.e. conformational change iv). The NSD analysis of the structures confirmed that the MCR protein matrix prevents F430 from deforming by an equal measure of ruffling and saddling [113].

Although inorganic molecular mechanics using crystal averaged metal parameters do not provide any electronic information, hole-size analysis [118–120] can be used to obtain an insight to the redox behavior of a bioinorganic complex. This was first shown by Hambley and co-workers who also pointed out the limitations of the technique [121,122]. Since low-spin Ni(II)–$N_{pyrrole}$ distances are typically between 1.85 and 1.91 Å, high-spin six-coordinate Ni(II)–$N_{pyrrole}$ distances are between 1.98 and 2.05 Å and six-coordinate Ni(I)–$N_{pyrrole}$ distances are even longer with Ni(I)–$N_{pyrrole}$ distances of about 2.1 Å, the hole-size of cofactor F430 will influence the redox potential of the coordinated nickel. MCR is a redox active protein in which the inactive nickel(II) form is reduced to the active nickel(I) species—we have therefore used MM based hole-size analysis to examine the effect MCR has on the hole-size of cofactor F430 [114].

In molecular mechanics, it is common practice to drive a certain parameter, for example, a torsion angle, through a series of fixed values to obtain the strain energy as a function of the parameter. A curve of the strain energy versus the M–N bond distance can similarly be obtained by systematically increasing the ideal M–N distance in the force field and calculating the strain after each increase. The minimum of such a graph occurs at the ideal M–N bond length, because the strain energy is at a minimum when the tetrapyrrole hole-size perfectly matches the metal size [118,119]. The ideal M–N bond length therefore represents the metal to nitrogen distance of a hypothetical metal that would best fit the ligand in its lowest energy conformation. As there is some controversy [25,123–127] about restraining versus constraining the M–N bonds, we did the calculations with a very weak, regular and very strong M–N force constant.

Fig. 4 shows the relative strain energy versus the imposed ideal metal to nitrogen distance curve obtained for six-coordinate cofactor F430 (triangles) and six-coordinate F430 in MCR (squares). According to the graph the ideal average M–N distance of six-coordinate metal ion in cofactor F430 is 2.06 Å. The same procedure was carried out with cofactor F430 in the active site of MCR. The ideal metal–nitrogen distance is 1.97 Å when F430 is in MCR.

The hole scan of F430 and F430 in MCR shows that F430 has a larger ideal Ni–N distance in solution than it does in the protein, and that the tetrapyrrole is more rigid in the protein, i.e. deviations from the ideal Ni–N distance cause more rapid increases of the relative strain energy and a steeper parabola. This narrowing of the ideal-metal distance caused by MCR imposing some rigidity upon F430 will affect the redox chemistry of MCR, since the nickel(II)/nickel(I) couple is associated with an increase in metal ion size.

In order to further examine the structural effects MCR imposes upon F430 as a function of its hole-size the non-planar defor-

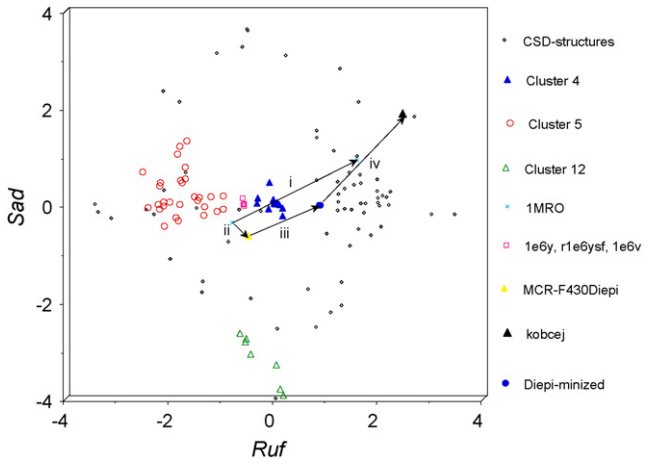

Fig. 3. B2u(sad) and B2u(ruf) deformations of all the tetrapyrrole structures in the Cambridge Structural Database and F430 in *Methanosarcina barkeri* and *Methanopyrus kandleri* MCR (□) clustered as described in reference [113]. A 1-Å distortion means that the square root of the sum of the squares of the *z*-displacements from the mean plane is equal to one [107]. Conformational changes shown are (i) F430 within MCR(1MRO) to free F430, (ii) F430 within MCR to 12,13-diepimerized F430 within the protein, (iii) 12,13-diepi F430 to free 12,13-diepi F430 minimized without a conformational search and (iv) free 12,13-diepi F430 minimized without a conformational search to the free 12,13-diepi F430M solid state structure [117].

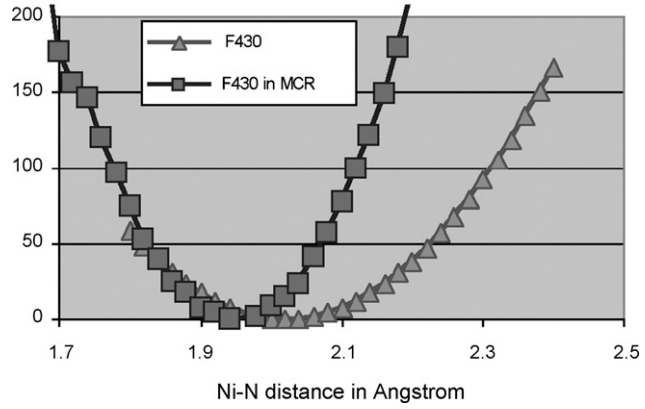

Fig. 4. Relative strain energy (kJ/mol) for a six-coordinate metal ion bound to F430 (▲), and for a six-coordinate metal ion bound to F430 in MCR (■), as a function of the ideal M–N bond length calculated as described by Hancock [118]. This graph has previously appeared in reference [114].

mations of cofactor-F430 were analyzed by normal-coordinate structural decomposition. The analysis [114] revealed that the surrounding protein has a significant effect on the non-planar deformations that the tetrahydrocorphinoid backbone of F430 undergoes in order to accommodate different metal sizes. In the absence of protein, F430 undergoes a significant ruffling deformation (>2 Å) to accommodate small metal ions (M–N < 1.90 Å), while increasing the ideal M–N distance results in a reduction in the amount of ruffling and an increase in the amount of saddling. Ruffling is also the predominant non-planar deformation F430 undergoes when it is inside MCR. However, F430 is able to undergo significantly less ruffling in the protein, and increasing the metal size results in a decrease in both ruffling and saddling.

Changing the coordination number of the nickel ion in F430 has a very small effect on the ideal hole-size, however, it has a significant effect on the non-planar deformations the coenzyme undergoes upon contraction and expansion. In all complexes, we examined cofactor F430 undergoes more non-planar deformations when it contains a four-cordinate metal ion than it does when it contains a six-coordinate metal ion.

It has been suggested that proteins are able to enforce unstable geometries, thereby producing an entatic state [128–131] that can increase the reactivity of the active site. Using molecular mechanical calculations to search the conformational space available to F430 and to do hole scans we have shown that MCR enforces an entatic state by favoring F430 over 12,13-diepi F430, and by moderating the non-planar deformations F430 can adopt.

2.2.2. Urease

Urease catalyzes the hydrolysis of urea to ammonia and carbamate, which is unstable and subsequently degrades to produce a second ammonia molecule and carbonic acid.

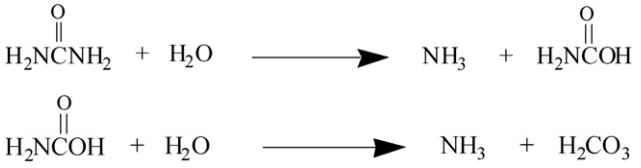

The catalyzed reaction is 1014 times the rate of the uncatalyzed reaction in which urea breaks down to ammonia and cyanic acid.

Urease has a dinickel active site. Based on the crystal structure of urease one of the nickel ions (Ni-1) was originally thought to be trigonally coordinated by His246, His272, Lys217, and the other (Ni-2) was thought to have a distorted trigonal bipyramidal or distorted square pyramidal geometry and be coordinated to Lys217, His134, His136, Asp360 and a water molecule [132]. The three coordinate pseudotetrahedral geometry initially proposed for the Ni-1 in urease is highly unusual and was cause for some concern to us. In parameterization, we therefore used different coordination geometries around Ni-1. The structure was minimized using three coordinate Ni-1, four coordinate Ni-1 with a water molecule bound to the fourth site, and four coordinate Ni-1 with a water molecule bridging Ni-1 and Ni-2. The best overlap, and the most accurate Ni–Ni distance was obtained with four coordinate Ni-1 and a bridging water molecule. This finding was corroborated by a Cambridge Structure Database (CSD) search, which showed that all structures with Ni–Ni distances of between 2.8 and 3.6 Å were bridged not only by a RCO_2 group but by an additional group like a water molecule. Complexes, like urease, with no Ni–Ni bonds and no additional bridging groups have Ni–Ni distances longer than 3.7 Å. We therefore proposed that an additional bridging group was present in urease since all carbonyl bridged nickel complexes in the CSD with Ni–Ni distances of between 2.8 and 3.6 Å have an additional bridging ligand [133,134]. Subsequently, the authors of the paper describing the original urease crystal structures reevaluated the electron density around the nickel ions in the structure and inserted two more waters in the active site, including a bridging water (or hydroxide) between the nickel ions. This was a validation of the ability of our parameters to model the solid state structure of urease, but was a serendipitous finding that could just as easily have been determined by DFT calculations.

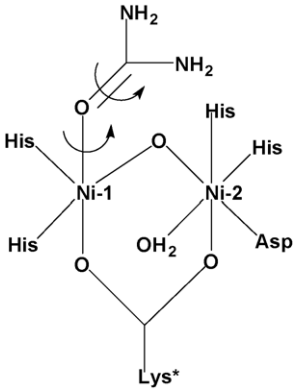

Fig. 5. The active site of *Klebsiella aerogenes* urease with urea bound to Ni-1 through it's oxygen atom. The N_{His272}–Ni-1–O–C_{urea} and Ni-1–O–C_{urea}–N_{urea} dihedrals were systematically rotated to obtain a Ramachandran plot.

The main reason we used inorganic MM calculations was to undertake a thorough conformational search to find the conformations available to nickel coordinated urea within urease. The structures of the wild-type binickel urease, the apoenzyme, acetohydroxamic acid inhibited urease and the mutants of *Klebsiella aerogenes* are all remarkably similar to each other and to the β-mercaptoethanol inhibited *Bacillus pasteurii* urease [135,136]. We therefore made the assumption that the active site of urease will not undergo a major conformational change upon binding urea, and that the wild-type crystal structure is a good starting point for molecular mechanics calculations.

A CSD search revealed that all nickel(II) solid state structures containing coordinated urea have the urea coordinating through its carbonyl carbon. If one therefore presumes that in urease the urea coordinates Ni-1 through its carbonyl oxygen, then there are two major variables influencing the orientation of the urea molecule in the active site of urease, they are the two dihedral angles shown in Fig. 5.

Three different conformational searches were undertaken to find the conformational space available to nickel-1 coordinated urea in urease.

(i) A Ramachandran type plot was generated by driving the dihedral angles shown in Fig. 1. From this plot, the ideal orientation of urea was determined to have a N_{His272}–Ni-1–O–C_{urea} dihedral angle of 207° and a Ni-1–O–C_{urea}–N_{urea} dihedral angle of 151°. The plot also indicates that the urea is located in a pocket within the urease and can adopt any conformation with a Ni-1–O–C_{urea}–N_{urea} dihedral angle of 0–360° if the N_{His272}–Ni-1–O–C_{urea} dihedral angle is around 240 ± 30°.

(ii) Conformational searches, in which only the position and the torsion angles of the urea itself were varied, were conducted using the Monte Carlo torsional and molecular position variation method [137,138]. All the low-energy conformations found in these searches were located in low-energy areas of the Ramachandran plot.

(iii) A Monte Carlo dihedral and translational conformational search was also undertaken in which all the variable dihedral angles of all the amino acid side-chains (His219, Glu220, Asp221, Leu316, Cys319, His320, Arg336 and Met364) within 8 Å of the urea and the dihedrals shown in Fig. 5, were randomly varied 10,000 times together with the position of Ni-1. Conformational searches of this type are able to find all the geometric isomers, conformations and configurations of inorganic complexes in one search [48]. All the low-energy conformations (3790 conformations) within 50 kJ/mol of the lowest energy minimum had urea conformations that were located in the low-energy valley found in the Ramachandran plot. A cluster analysis of all residues within 8 Å of the urea revealed that most of the low-energy structures were located in a large cluster which had the same hydrogen-bonding pattern. This hydrogen-bonding pattern is not part of any of the proposed mechanisms for the degradation of urea by urease.

Since the Monte Carlo dihedral and translational conformational search varied all the side chains in the vicinity of the urea and found the same low-energy areas as those located in the Ramachandran plot this confirms that the Ramachandran plot is a valid tool in this case, and that rotating the urea dihedral angles does not cause the surrounding residues to adopt a new conformation that was not found without a conformational search. Ramachandran plots, with active sites and protonation states modified to model the different urease mechanisms, were subsequently used to evaluate these different mechanisms. Based upon the low-energy conformations available to urea in the active site of wild-type urease one can conclude that the traditional "His320 acts as a base" mechanism is unlikely, while the N,O urea bridged and the reverse protonation mechanisms cannot be ruled out. However, the hydrogen-bonding network present in all the low-energy conformations found in the Monte Carlo dihedral and translational conformational search was not part of any of the mechanisms proposed mechanisms [139]. Subsequent experimental studies [140,141] have reinforced the need for a new alternative mechanism for urea degradation by urease and a new one has been proposed—the cyanate intermediate mechanism.

Recently, high level QM and DFT calculations [142–144] were used to analyze equilibrium geometries, electronic properties, kinetics and energies for a series of urease active site models. Both hydroylytic and elimination mechanisms are possible according to these calculations. The same researchers also undertook a mammoth molecular dynamics simulation of the complete urease trimer (2479 residues) [145]. The MD simulations revealed several pathways were possible as different hydrogen-bonding networks were present depending on the point in the simulation and on the specific active site studied.

3. Final remarks

Inorganic and bioinorganic molecular mechanics calculations are fairly rare, particularly in comparison to bioorganic and organic calculations. The main reasons for this are that electronic effects due to partially occupied d-orbitals are very important in the chemistry of transition metal ions, and that there is no force field able to model most, or even some, metal ions in all their different redox states and coordination geometries. In order to undertake inorganic molecular mechanical calculations parameters for the metal coordination sphere need to be determined, this is a significant activation barrier to undertaking inorganic molecular mechanics calculations. Once parameters have been determined care needs to be taken not to overinterpret the results obtained [96]. Despite all these drawbacks inorganic MM calculations still have a role in modern computational bioinorganic chemistry. They are fast, which means that they can be used to model large systems or to do many calculations. In this review, we have shown examples where we have used MM calculations because they have allowed us to undertake a thorough conformational search of the extended nickel coordination sphere in both methyl coenzyme-M reductase and urease. In most cases, such as the ones presented its advantageous to use additional methods, such as normal-coordinate structural decomposition, database and cluster analysis to interpret and/or confirm the results of the calculations.

References

[1] F. Neese, Journal of Biological Inorganic Chemistry 11 (2006) 702.
[2] B. Kirchner, F. Wennmohs, S.F. Ye, F. Neese, Current Opinion in Chemical Biology 11 (2007) 134.
[3] A. Ghosh, Journal of Biological Inorganic Chemistry 11 (2006) 671.
[4] P.E.M. Siegbahn, Journal of Biological Inorganic Chemistry 11 (2006) 695.
[5] P.E.M. Siegbahn, T. Borowski, Accounts of Chemical Research 39 (2006) 729.
[6] E.M. Sproviero, J.A. Gascon, J.P. McEvoy, G.W. Brudvig, V.S. Batista, Journal of the American Chemical Society 130 (2008) 3428.
[7] E.M. Sproviero, J.A. Gascon, J.P. McEvoy, G.W. Brudvig, V.S. Batista, Coordination Chemistry Reviews 252 (2008) 395.
[8] H.M. Senn, W. Thiel, Current Opinion in Chemical Biology 11 (2007) 182.
[9] H.M. Senn, W. Thiel, Atomistic Approaches in Modern Biology: from Quantum Chemistry to Molecular Simulations, in: Topics in Current Chemistry, vol. 268, Springer-Verlag, Berlin, 2007, p. 173.
[10] J. Heimdal, P. Rydberg, U. Ryde, Journal of Physical Chemistry B 112 (2008) 2501.
[11] J.-P. Mathieu, Annals of Physics 19 (1944) 335.
[12] E.J. Corey, J.C. Bailar, Journal American Chemical Society 81 (1959) 2620.
[13] P. Comba, T. Hambley, Molecular Modeling of Inorganic Compounds, VCH, Weinheim, 2000.
[14] R.J. Deeth, N. Fey, B. Williams-Hubbard, Journal of Computational Chemistry 26 (2005) 123.
[15] R.J. Deeth, Inorganic Chemistry 46 (2007) 4492.
[16] N. Gresh, J. Sponer, Journal of Physical Chemistry B 103 (1999) 11415.
[17] N. Gresh, G.A. Cisneros, T.A. Darden, J.P. Piquemal, Journal of Chemical Theory and Computation 3 (2007) 1960.
[18] T.K. Firman, C.R. Landis, Journal of the American Chemical Society 123 (2001) 11728.
[19] C. Landis, T. Cleveland, T. Firman, JACS 120 (1998) 2639.
[20] P. Comba, R. Remenyi, Coordination Chemistry Reviews 238 (2003) 9.
[21] R.J. Deeth, Coordination Chemistry Reviews 212 (2001) 11.
[22] J.P. Piquemal, B. Williams-Hubbard, N. Fey, R.J. Deeth, N. Gresh, C. Giessner-Prettre, Journal of Computational Chemistry 25 (2004) 308.
[23] T. Hambley, C. Hawkins, J. Palmer, M. Snow, Australian Journal of Chemistry 34 (1981) 45.
[24] D.L. Kepert, Inorganic Stereochemistry, Springer Verlag, Heidelberg, 1982.
[25] P. Comba, T.W. Hambley, M. Bodo, Molecular Modeling of Inorganic Compounds, Wiley-VCH, Weinheim, 2008.
[26] D.A. Case, T.E. Cheatham, T. Darden, H. Gohlke, R. Luo, K.M. Merz, A. Onufriev, C. Simmerling, B. Wang, R.J. Woods, Journal of Computational Chemistry 26 (2005) 1668.
[27] N. Allinger, Y. Yuh, J. Lii, JACS 111 (1989) 8551.
[28] T.A. Halgren, Journal of Computational Chemistry 17 (1996) 490.
[29] W. Damm, T.A. Halgren, R.B. Murphy, A.M. Smondyrev, R.A. Friesner, W.L. Jorgensen, Abstracts of Papers of the American Chemical Society 224 (2002) U471.
[30] W.L. Jorgensen, K.P. Jensen, A.N. Alexandrova, Journal of Chemical Theory and Computation 3 (2007) 1987.
[31] P. Comba, Inorganic Chemistry 33 (1994) 4577.
[32] J. Bol, C. Buning, P. Comba, J. Reedijk, M. Stroehle, Journal of Computational Chemistry 19 (1998) 512.
[33] P. Comba, K. Gloe, K. Inoue, T. Krueger, H. Stephan, K. Yoshizuka, Inorganic Chemistry 37 (1998) 3310.
[34] K. Born, P. Comba, A. Daubinet, A. Fuchs, H. Wadepohl, Journal of Biological Inorganic Chemistry 12 (2007) 36.
[35] C.E. Skopec, I. Cukrowski, H.M. Marques, Journal of Molecular Structure 783 (2006) 21.
[36] C.E. Skopec, J.M. Robinson, I. Cukrowski, H.M. Marques, Journal of Molecular Structure 738 (2005) 67.
[37] A.S. De Sousa, M.A. Fernandes, W. Nxumalo, J.L. Balderson, T. Jeftic, I. Cukrowski, H.M. Marques, Journal of Molecular Structure 872 (2008) 47.
[38] I. Kolossvary, G. WC, Journal of the American Chemical Society 118 (1996) 5011.
[39] H. Senderowitz, F. Guarnieri, W. Still, Journal of the American Chemical Society 117 (1995) 8211.
[40] G.M. Keseru, I. Kolossvary, Journal of the American Chemical Society 123 (2001) 12708.

[41] I. Kolossvary, G.M. Keseru, Journal of Computational Chemistry 22 (2001) 21.
[42] R.A. da Silva, L. Degreve, A. Caliri, Biophysical Journal 87 (2004) 1567.
[43] E. Leontidis, J.J. Depablo, M. Laso, U.W. Suter, Atomistic Modeling of Physical Properties, in: Advances In Polymer Science, vol. 116, Springer-Verlag, Berlin, 1994, p. 283.
[44] T. Yui, K. Ogawa, Trends in Glycoscience and Glycotechnology 17 (2005) 159.
[45] C.v.d. Lieth, T. Kozar, W. Hull, THEOCHEM Journal of Molecular Structure 395 (1997) 225.
[46] A. Treasurywala, E. Jaeger, M. Peterson, Journal of Computational Chemistry 17 (1996) 1171.
[47] J. Meza, R. Judson, T. Faulkner, A. Teasurywala, Journal of Computational Chemistry 17 (1996) 1142.
[48] J. Bartol, P. Comba, M. Melter, M. Zimmer, Journal of Computational Chemistry 20 (1999) 1549.
[49] G. Rosenblum, S. Meroueh, M. Toth, J.F. Fisher, R. Fridman, S. Mobashery, I. Sagi, Journal of the American Chemical Society 129 (2007) 13566.
[50] S. Hoops, K. Anderson, K.M. Merz, JACS 113 (1991) 8262.
[51] M.A. Garcia, S. Martin-Santamaria, A. Ramos, B. De Pascual-Teresa, Anales De La Real Academia Nacional De Farmacia 73 (2007) 703.
[52] M.C. Durrant, Biochemistry 43 (2004) 6030.
[53] M.C. Durrant, Biochemistry 41 (2002) 13934.
[54] M.C. Durrant, Biochemistry 41 (2002) 13946.
[55] M.C. Durrant, Biochemical Journal 355 (2001) 569.
[56] P. del Pino, W. Andreas, U. Bertsch, C. Renner, M. Mentler, K. Grantner, F. Fiorino, W. Meyer-Klaucke, L. Moroder, H.A. Kretzschmar, F.G. Parak, European Biophysics Journal with Biophysics Letters 36 (2007) 239.
[57] M. Mentler, A. Weiss, K. Grantner, P. del Pino, D. Deluca, S. Fiori, C. Renner, W.M. Klaucke, L. Moroder, U. Bertsch, H.A. Kretzschmar, P. Tavan, F.G. Parak, European Biophysics Journal with Biophysics Letters 34 (2005) 97.
[58] A. Weiss, P. del Pino, U. Bertsch, C. Renner, M. Mender, K. Grantner, L. Moroder, H.A. Kretzschmar, F.G. Parak, Veterinary Microbiology 123 (2007) 358.
[59] T. Miura, S. Sasaki, A. Toyama, H. Takeuchi, Biochemistry 44 (2005) 8712.
[60] C.E. Ergenekan, D. Thomas, J.T. Fischer, M.L. Tan, M.K. Eidsness, C.H. Kang, T. Ichiye, Biophysical Journal 85 (2003) 2818.
[61] P.D. Swartz, B.W. Beck, T. Ichiye, Biophysical Journal 71 (1996) 2958.
[62] R.B. Yelle, N.S. Park, T. Ichiye, Proteins-Structure Function and Genetics 22 (1995) 154.
[63] N. Gresh, P. Derreumaux, Journal of Physical Chemistry B 107 (2003) 4862.
[64] P. Derreumaux, Physical Review Letters 85 (2000) 206.
[65] P. Derreumaux, Journal of Chemical Physics 117 (2002) 3499.
[66] W.F. Li, J. Zhang, J. Wang, W. Wang, Journal of the American Chemical Society 130 (2008) 892.
[67] K.E.R. Duncan, M.J. Stillman, Journal of Inorganic Biochemistry 100 (2006) 2101.
[68] K.E. Rigby, J. Chan, J. Mackie, M.J. Stillman, Proteins-Structure Function and Bioinformatics 62 (2006) 159.
[69] J. Chan, Z. Huang, I. Watt, P. Kille, M.J. Stillman, Canadian Journal of Chemistry-Revue Canadienne De Chimie 85 (2007) 898.
[70] M.C. Durrant, A. Francis, D.J. Lowe, W.E. Newton, K. Fisher, Biochemical Journal 397 (2006) 261.
[71] R.E. Bongini, S.B. Culver, K.M. Elkins, Journal of Inorganic Biochemistry 101 (2007) 1251.
[72] A. Oda, N. Yamaotsu, S. Hirono, Journal of Computational Chemistry 26 (2005) 818.
[73] H.M. Marques, K. Brown, Journal of Molecular Structure 340 (1995) 97.
[74] H. Marques, C. Warden, M. Monye, M. Shongwe, K. Brown, Inorganic Chemistry 37 (1998) 2578.
[75] C.B. Perry, K.L. Brown, X. Zou, H.A. Marques, Journal of Molecular Structure 737 (2005) 245.
[76] K.L. Brown, H.M. Marques, THEOCHEM Journal of Molecular Structure 714 (2005) 209.
[77] C. Bauer, B. Jaun, Helvetica Chimica Acta 86 (2003) 4233.
[78] C. Bauer, B. Jaun, Helvetica Chimica Acta 86 (2003) 4254.
[79] S.R. Niketic, K. Rasmussen, The Consistent Force Field: A Documentation, Springer-Verlag, Berlin-Heidelberg, 1977.
[80] S. Niketic, K. Rasmussen, Acta Chemica Scandinavia A32 (1978) 391.
[81] S. Niketic, K. Rasmussen, Acta Chemica Scandinavica A35 (1981) 213.
[82] N. Raos, S. Niketic, V. Simeon, Journal of Inorganic Biochemistry 16 (1982) 1.
[83] S. Zaric, S.R. Niketic, Polyhedron 10 (1991) 2665.
[84] M. Gruden, S. Grubisic, A.G. Coutsolelos, S.R. Niketic, Journal of Molecular Structure 595 (2001) 209.
[85] S. Grubisic, M.K. Milicic, D.D. Radanovic, S.R. Niketic, Journal of Molecular Structure 794 (2006) 125.
[86] M. Gruden-Pavlovic, S. Grubisic, S.R. Niketic, Journal of Inorganic Biochemistry 98 (2004) 1293.
[87] M. Gruden-Pavlovic, S. Grubisic, M. Zlatar, S.R. Niketic, International Journal of Molecular Sciences 8 (2007) 810.
[88] K. Spiegel, A. Magistrato, P. Maurer, P. Ruggerone, U. Rothlisberger, P. Carloni, J. Reedijk, M.L. Klein, Journal of Computational Chemistry 29 (2008) 38.
[89] N. Gresh, J.E. Sponer, N. Spackova, J. Leszczynski, J. Sponer, Journal of Physical Chemistry B 107 (2003) 8669.
[90] A. Magistrato, P. Ruggerone, K. Spiegel, P. Carloni, J. Reedijk, Journal of Physical Chemistry B 110 (2006) 3604.
[91] N. Gresh, Journal of Computational Chemistry 16 (1995) 856.
[92] N. Gresh, D.R. Garmer, Journal of Computational Chemistry 17 (1996) 1481.
[93] U. El-Ayaan, A.A.M. Abdel-Aziz, S. Al-Shihry, European Journal of Medicinal Chemistry 42 (2007) 1325.
[94] L. Petraccone, E. Erra, A. Messere, D. Montesarchio, G. Piccialli, G. Barone, C. Giancola, Biophysical Chemistry 104 (2003) 259.
[95] M. Zimmer, Chemical Reviews 95 (1995) 2629.
[96] P. Comba, M. Zimmer, Journal of Chemical Education 73 (1996) 108.
[97] J.G. Ferry, Science 278 (1997) 1413.
[98] W. Grabarse, F. Mahlert, E.C. Duin, M. Goubeaud, S. Shima, R.K. Thauer, V. Lamzin, U. Ermler, Journal of Molecular Biology 309 (2001) 315.
[99] W.G. Grabarse, F. Mahlert, S. Shima, R.K. Thauer, U. Ermler, Journal of Molecular Biology 303 (2000) 329.
[100] U. Ermler, W. Grabarse, S. Shima, M. Goubeaud, R.K. Thauer, Science 278 (1997) 1457.
[101] V. Pelmenschikov, M.R.A. Blomberg, P.E.M. Siegbahn, R.H. Crabtree, Journal of the American Chemical Society 124 (2002) 4039.
[102] U. Ermler, W. Grabarse, S. Shima, M. Goubeaud, R.K. Thauer, Current Opinion in Structural Biology 8 (1998) 749.
[103] A. Pfaltz, D.A. Livingston, B. Jaun, G. Diekert, R.K. Thauer, A. Eschenmoser, Helvetica Chimica Acta 68 (1985) 1338.
[104] G. Farber, W. Keller, C. Kratky, B. Jaun, A. Pfaltz, C. Spinner, A. Kobelt, A. Eschenmoser, Helvetica Chimica Acta 74 (1991) 697.
[105] F.H. Allen, Acta Crystallographica Section B-Structural Science 58 (2002) 380.
[106] M. Zimmer, Journal Biomolecular Structure and Dynamics 11 (1993) 203.
[107] J.A. Shelnutt, X.Z. Song, J.G. Ma, S.L. Jia, W. Jentzen, C.J. Medforth, Chemical Society Reviews 27 (1998) 31.
[108] K.M. Barkigia, L. Chantranupong, K.M. Smith, J. Fajer, Journal of the American Chemical Society 110 (1988) 7566.
[109] m. Ravikanth, T. Chandrashekar, Structure and Bonding 82 (1995) 107.
[110] C.M. Drain, C. Kirmaier, C.J. Medforth, D.J. Nurco, K.M. Smith, D. Holten, Journal of Physical Chemistry 100 (1996) 11984.
[111] S. Othman, J. Fitch, M.A. Cusonovich, A. Desbois, Biochemistry 36 (1997) 5499.
[112] Q. Tang, P.E. Carrington, Y.C. Horng, M.J. Maroney, S.W. Ragsdale, D.F. Bocian, Journal of the American Chemical Society 124 (2002) 13242.
[113] L.N. Todd, M. Zimmer, Inorganic Chemistry 41 (2002) 6831.
[114] C. Mbofana, M. Zimmer, Inorganic Chemistry 45 (2006) 2598.
[115] J.A. Shelnutt, in: K.M. Kadish, K.M. Smith, R. Guilard (Eds.), The Porphyrin Handbook, Academic Press, 2000.
[116] W. Jentzen, X. Song, J. Shelnutt, Journal of Physical Chemistry 101 (1997) 1684.
[117] C.F. Kratky, A.A. Pfaltz, B. Krautler, B. Jaun, A. Eschenmoser, Journal of the Chemical Society, Chemical Communications 1984 (1984) 1368.
[118] R.D. Hancock, Progress in Inorganic Chemistry 37 (1989) 188.
[119] C. Canales, L. Egan, M. Zimmer, Journal of Chemical Education 69 (1992) 21.
[120] H. De Bari, M. Zimmer, Inorganic Chemistry 43 (2004) 3344.
[121] A.M. Bond, T.W. Hambley, M.R. Snow, Inorganic Chemistry 24 (1985) 1920.
[122] P. Comba, T.W. Hambley, P. Hilfenhaus, D.T. Richens, Journal of the Chemical Society-Dalton Transactions (1996) 533.
[123] R. Hancock, P. Wade, M. Ngwenya, A. de Sousa, K. Damu, Inorganic Chemistry 29 (1990) 1968.
[124] P. Comba, Coordination Chemistry Reviews 123 (1993) 1.
[125] M. Drew, P. Yates, Journal of the Chemical Society, Dalton Transactions (1986) 2506.
[126] R. Hancock, M. Drew, P. Yates, Journal of the Chemical Society, Dalton Transactions 1986 (1986) 2505.
[127] P. Comba, Coordination Chemistry Reviews 185–186 (1999) 81.
[128] R.J.P. Williams, Journal of Molecular Catalysis 30 (1985) 1.
[129] R.J.P. Williams, European Journal of Biochemistry 234 (1995) 363.
[130] P. Comba, Coordination Chemistry Reviews 200 (2000) 217.
[131] P. Comba, W. Schiek, Coordination Chemistry Reviews 238 (2003) 21.
[132] E. Jabri, M.B. Carr, R. Hausinger, A. Karplus, Science 268 (1995) 998.
[133] C. Csiki, K.M. Norenberg, C.M. Shoemaker, M. Zimmer, in: L. Banci, P. Comba (Eds.), NATO Advanced Research Workshop on Molecular Modeling and Dynamics of Biological Molecules Containing Metal Ions, vol. 41, Kluwer, San Miniato, Italy, 1997, p. 105.
[134] C. Csiki, M. Zimmer, Journal of Biomolecular Structure and Dynamics 17 (1999) 121.
[135] S. Benini, S. Ciurli, W. Rypnieiewski, K. Wilson, S. Mangani, Acta Crystallographica Section D D54 (1998) 409.
[136] S. Benini, W.R. Rypniewski, K.S. Wilson, S. Mangani, S. Ciurli, Journal of the American Chemical Society 126 (2004) 3714.
[137] G. Chang, W.C. Guida, W.C. Still, Journal of the American Chemical Society 111 (1989) 4379.
[138] M. Saunders, K. Houk, Y.-D. Wu, C. Still, M. Lipton, G. Chang, W. Guida, JACS 112 (1990) 1419.
[139] M. Zimmer, Journal of Biomolecular Structure and Dynamics 17 (2000) 787.
[140] A.M. Barrios, S.J. Lippard, Inorganic Chemistry 40 (2001) 1250.
[141] A.M. Barrios, S.J. Lippard, Journal of the American Chemical Society 122 (2000) 9172.
[142] G. Estiu, K.M. Merz, Journal of the American Chemical Society 126 (2004) 6932.
[143] D. Suarez, N. Diaz, K.M. Merz, Journal of the American Chemical Society 125 (2003) 15324.
[144] G. Estiu, K.M. Merz, Journal of Physical Chemistry B 111 (2007) 10263.
[145] G. Estiu, K.M. Merz, Biochemistry 45 (2006) 4429.